

Product measurements and fully symmetric measurements in qubit-pair tomography: A numerical study[☆]

TEO Yong Siah^{a,b,c}, ZHU Huangjun^{a,c}, Berthold-Georg ENGLERT^{a,b}

^a*Centre for Quantum Technologies, National University of Singapore, Singapore 117543, Singapore*

^b*Department of Physics, National University of Singapore, Singapore 117542, Singapore*

^c*NUS Graduate School for Integrative Sciences and Engineering, Singapore 117597, Singapore*

Abstract

State tomography on qubit pairs is routinely carried out by measuring the two qubits separately, while one expects a higher efficiency from tomography with highly symmetric joint measurements of both qubits. Our numerical study of simulated experiments does not support such expectations.

Key words: quantum state tomography, positive operator measurement, symmetric informationally complete measurement

PACS: 03.65.Ud, 03.65.Wj, 03.67.-a

1. Introduction

Quantum state tomography makes efficient use of the resources if it employs a probability operator measurement (POM) with the minimal number of outcomes — $4 = 2^2$ for single-qubit tomography, $16 = 4^2$ for qubit-pair tomography, d^2 for tomography in a d -dimensional Hilbert space. Ideally, one would like to acquire tomographic data with the aid of a symmetric informationally complete (SIC) measurement [1, 2] because it probes the state space in an unbiased way and promises minimal statistical errors on average when many, uniformly distributed, quantum states are measured [3, 4].

The SIC tetrahedron measurement [3, 5] has been implemented for polarization qubits of single photons [6, 7], and the product POM that is composed of the joint measurements of two single-qubit SIC POMs has been used successfully for two-qubit state tomography [8]. This product POM is, however, not a SIC POM for the qubit pair, which invites the question whether the realization of the two-qubit SIC POM, with its challenge of implementing projections to entangled states, is worth the effort. Our answer is: Hardly.

The evidence that justifies this answer is numerical. We generate simulated tomographic data, both for the product POM and the SIC POM, for two-qubit states that are chosen either specifically or randomly. Then we estimate the state from the simulated data and compare the reconstructed state with the pre-chosen true state. The figure of merit is the trace-class distance between the two states.

The paper is organized as follows. We introduce notation and terminology in Sec. 2 where we briefly review schemes for state tomography. Then, in Sec. 3, we remark on group covariant SIC POMs and specify the product POM and SIC POM that we use for the numerical study. Its ingredients — state estimation and the generation of random samples of states — are described in Secs. 4 and 5, respectively. The results of the simulated experiments are presented in Sec. 6 for tomography of maximally entangled states, and in Sec. 7 for averages over random samples of states. We close with offering our conclusion in Sec. 8.

[☆]We dedicate this work to the memory of Krzysztof Wódkiewicz, a friend and colleague who left us much too early.

2. Measurement schemes for state tomography

A POM¹ is a decomposition of the identity into J probability operators Π_j , which we call *outcomes*,

$$\sum_{j=0}^{J-1} \Pi_j = 1 \quad \text{with} \quad \Pi_j > 0. \quad (1)$$

The probabilities

$$p_j = \text{tr}\{\rho\Pi_j\} \quad \text{with} \quad \sum_{j=0}^{J-1} p_j = 1 \quad (2)$$

permit a reconstruction of the statistical operator ρ , the *state* of the physical system, if the POM is informationally complete (IC). In a d -dimensional Hilbert space, an IC POM must have at least d^2 outcomes, and a minimal IC POM has exactly $J = d^2$ outcomes and no redundant ones, and then the state ρ is uniquely expressed in terms of the probabilities p_j and the *reconstruction operators* P_j that are dual to the outcomes Π_j ,

$$\rho = \sum_{j=0}^{d^2-1} p_j P_j, \quad \text{where} \quad \text{tr}\{P_j\Pi_k\} = \delta_{jk}. \quad (3)$$

A SIC POM is a minimal IC POM with the symmetry property that all outcomes are unitarily equivalent with “equal angles” between each pair of outcomes,

$$\begin{aligned} \text{tr}\{\Pi_j\Pi_k\} = a\delta_{jk} + b & \quad \text{with} \quad \text{tr}\{\Pi_j\} = a + bd^2 = \frac{1}{d} \\ \text{and} \quad \frac{1}{d^3} < \text{tr}\{\Pi_j^2\} = a + b & \leq \frac{1}{d^2}. \end{aligned} \quad (4)$$

The reconstruction operators for such a SIC POM are

$$P_j = \frac{1}{a}(\Pi_j - bd), \quad (5)$$

so that

$$\text{tr}\{P_j\} = 1, \quad \text{tr}\{P_j P_k\} = \frac{1}{a}(\delta_{jk} - bd), \quad \sum_{j=0}^{d^2-1} P_j = d. \quad (6)$$

These translate $d^{-1} \leq \text{tr}\{\rho^2\} \leq 1$ into

$$\sum_{j=0}^{d^2-1} \left(p_j - \frac{1}{d^2}\right)^2 \leq \frac{d-1}{d} a, \quad (7)$$

a second constraint obeyed by the probabilities p_j in addition to the unit sum in (2). The equal sign in (7) applies when ρ is a pure state, $\rho^2 = \rho$, and only then.

When the d^2 outcomes Π_j of a SIC POM are rank-1 operators, that is: when they are subnormalized projectors to pure states, then $a + b$ assumes the maximal value permitted by (4),

$$\begin{aligned} \text{rank-1 SIC POM:} \quad a + b = \frac{1}{d^2}, \quad a = bd = \frac{1}{d + d^2}, \\ \Pi_j^2 = \frac{1}{d}\Pi_j, \quad P_j = (d + d^2)\Pi_j - 1. \end{aligned} \quad (8)$$

Almost all SIC POMs studied in the published literature are of this rank-1 kind. One exception is the two-qubit SIC POM of Ref. [9] whose rank-3 outcomes are optimal entanglement witnesses. In the present context, we will only deal with standard rank-1 SIC POMs.

¹POM, with its emphasis on “probability” and “measurement” is quantum physics jargon. The corresponding popular mathematical term POVM (positive-operator valued measure) makes reference to measure theory.

3. Group covariant SIC POMs and their fiducial states

As conjectured in [1, 2], for every Hilbert space dimension d , there exist rank-1 SIC POMs which are covariant with respect to the Heisenberg–Weyl group, also called the generalized Pauli group because it is the d -dimensional analog of the $d = 2$ group of unitary transformations effected by the Pauli operators σ_x , σ_z and their products, including $\sigma_x\sigma_z = -i\sigma_y$ as well as the identity $\sigma_x^2 = 1$. Indeed, SIC POMs of this group covariant kind are typical.

The Heisenberg–Weyl group refers to a pre-chosen basis of kets $|0\rangle, |1\rangle, \dots, |d-1\rangle$. They are eigenkets of the d -periodic unitary operator Z , the analog of σ_z ,

$$Z|k\rangle = |k\rangle e^{i2\pi k/d}, \quad Z^d = 1, \quad (9)$$

and are cyclically permuted by the d -periodic unitary operator X , the analog of σ_x ,

$$X|k\rangle = |k+1\rangle \quad \text{for } k = 0, 1, \dots, d-2, \quad X|d-1\rangle = |0\rangle, \quad X^d = 1. \quad (10)$$

The (m, n) th element in the abelian Heisenberg–Weyl group of unitary transformations is the mapping

$$F \rightarrow X^m Z^n F Z^{-n} X^{-m} = Z^n X^m F X^{-m} Z^{-n} \\ \text{for } m, n = 0, 1, \dots, d-1, \quad (11)$$

where F is any linear operator on the d -dimensional Hilbert space of kets. Although X and Z do not commute, $ZX = e^{i2\pi/d} XZ$, the order of factors does not matter in the transformation (11), and so we have d^2 group elements.

A group covariant SIC POM is composed of the outcomes

$$\Pi_{mn} = X^m Z^n \Pi_{00} Z^{-n} X^{-m}, \quad (12)$$

where the d^2 pairs m, n take over the role of label j in (4) and Π_{00} is the *fiducial outcome*. The ergodic property of the Heisenberg–Weyl group,

$$\sum_{m,n=0}^{d-1} X^m Z^n F Z^{-n} X^{-m} = d \operatorname{tr}\{F\}, \quad (13)$$

ensures that the Π_{mn} s are proper outcomes of a POM if Π_{00} is a probability operator with $\operatorname{tr}\{\Pi_{00}\} = 1/d$. But the rank-1 SIC POM condition of (4) with a and b from (8) is obeyed only if $\Pi_{00} = |f\rangle d^{-1} \langle f|$ is such that

$$|\langle f|X^m Z^n|f\rangle|^2 = \frac{1 + d \delta_{m0} \delta_{n0}}{1 + d} \quad \text{for } m, n = 0, 1, \dots, d-1, \quad (14)$$

where the normalized $|f\rangle$ is the fiducial ket or *seed* [2]. The set of equations (14) can serve as the basis for a numerical search, successfully completed by Renes *et al.* up to $d = 45$ [2], but there are also analytically known fiducial kets and their rank-1 POMs.

For the qubit case $d = 2$, we have the familiar *tetrahedron measurement* with the outcomes

$$T_0 = \frac{1}{4\sqrt{3}}(\sqrt{3} + \sigma_x + \sigma_y + \sigma_z), \\ T_1 = \frac{1}{4\sqrt{3}}(\sqrt{3} + \sigma_x - \sigma_y - \sigma_z) = \sigma_x T_0 \sigma_x, \\ T_2 = \frac{1}{4\sqrt{3}}(\sqrt{3} - \sigma_x - \sigma_y + \sigma_z) = \sigma_z T_0 \sigma_z, \\ T_3 = \frac{1}{4\sqrt{3}}(\sqrt{3} - \sigma_x + \sigma_y - \sigma_z) = \sigma_x \sigma_z T_0 \sigma_z \sigma_x, \quad (15)$$

for which

$$\sum_{j=0}^3 T_j = 1, \quad \text{tr}\{T_j\} = \frac{1}{2}, \quad \text{tr}\{T_j T_k\} = \frac{1}{6}\delta_{jk} + \frac{1}{12}. \quad (16)$$

Its name derives from the geometry of the four Pauli vectors \vec{t}_j ,

$$T_j = \frac{1}{4}(1 + \vec{t}_j \cdot \vec{\sigma}), \quad \vec{t}_j \cdot \vec{t}_k = \frac{4}{3}\delta_{jk} - \frac{1}{3}, \quad (17)$$

whose tips are the corners of a tetrahedron inside the Bloch sphere. See Ref. [3] for the properties of the tetrahedron measurement, and Ref. [6] for its implementation for experimental tomography of photon polarization qubits.

The tensor product of two tetrahedron SIC POMs,

$$T_{mn} = T_m \otimes T_n, \quad \sum_{m,n=0}^3 T_{mn} = 1, \quad (18)$$

is a perfectly suitable POM for two-qubit tomography. It is central to the Singapore protocol for quantum key distribution [10], and has been used in the experiments by Ling *et al.* [8]. This product POM is, however, not a SIC POM for the qubit pair.

For two-qubit SIC tomography, we can use any one of the known SIC POMs for $d = 4$, but they are not equivalent in their two-qubit properties, such as the concurrence of the outcomes [11]. We prefer a particular SIC POM, generated from Appelby's fiducial state [12],

$$|f_A\rangle = (|00\rangle, |01\rangle, |10\rangle, |11\rangle) \frac{1}{2\sqrt{3+G}} \begin{pmatrix} 1 + e^{-i\pi/4} \\ e^{i\pi/4} + iG^{-3/2} \\ 1 - e^{-i\pi/4} \\ e^{i\pi/4} - iG^{-3/2} \end{pmatrix}, \quad (19)$$

where $G = (\sqrt{5} - 1)/2$ is the golden ratio. The transformations of the Heisenberg–Weyl group refer to the two-qubit kets $|j_1 j_2\rangle = |j_1\rangle \otimes |j_2\rangle$ in the order stated, so that we have

$$Z = \frac{1+i}{2}\sigma_z \otimes (1 - i\sigma_z), \quad X = \frac{1}{2}(1 + \sigma_x) \otimes \sigma_x - \frac{i}{2}(1 - \sigma_x) \otimes \sigma_y \quad (20)$$

for the two-qubit versions of the basic unitary operators in (9) and (10).

The outcomes Π_{mn} of the particular SIC POM that we get from the seed (19),

$$\Pi_{mn} = X^m Z^n |f_A\rangle \frac{1}{d} \langle f_A | Z^{-n} X^{-m} \quad \text{for } m, n = 0, 1, 2, 3, \quad (21)$$

possess an additional symmetry: all the 16 two-qubit states $d\Pi_{mn}$ have the same concurrence of $\sqrt{2/5}$. These two-qubit states are typical in the sense that their squared concurrence equals the average squared concurrence of all pure two-qubit states [13]. As a consequence of the common concurrence, one can turn the Π_{mn} s into each other with the aid of *local* unitary transformations that act on one of the qubits only. This is a rather peculiar feature, not shared by other SIC POMs for qubit pairs [11].

4. Techniques for state estimation

The data acquired in the simulated experiments are simply the counts of clicks of each of the 16 detectors, one for each outcome of the two-qubit POMs — the product POM of (18) and the SIC POM of (19) and (21). Owing to the statistical fluctuations that originate in the quantum indeterminism, the relative frequencies

of detector counts are not equal to the probabilities $p_{mn}^{(\text{prod})} = \text{tr}\{\rho T_{mn}\}$ and $p_{mn}^{(\text{SIC})} = \text{tr}\{\rho \Pi_{mn}\}$, at best the respective relative frequencies $\tilde{p}_{mn}^{(\text{prod})}$ and $\tilde{p}_{mn}^{(\text{SIC})}$ approximate the intrinsic probabilities.

Therefore, there is danger in relying on (3). The reconstructed states

$$\begin{aligned}\rho_{\text{est}}^{(\text{prod})} &= \sum_{m,n=0}^3 \tilde{p}_{mn}^{(\text{prod})} (6T_m - 1) \otimes (6T_n - 1), \\ \rho_{\text{est}}^{(\text{SIC})} &= \sum_{m,n=0}^3 \tilde{p}_{mn}^{(\text{SIC})} (20\Pi_{mn} - 1)\end{aligned}\quad (22)$$

are not guaranteed to be positive operators. It is possible, and indeed happens regularly when the true state has high purity, that these *raw data* (RD) estimates have negative eigenvalues because the relative frequencies do not obey restrictions such as the appropriate version of (7). In the context of single-qubit tomography with the tetrahedron measurement, this matter is discussed in section IV C of Ref. [3]. A thorough coverage of many aspects of quantum state estimation is given in the 2004 monograph of Paris and Řeháček [14].

The probability that a total of N detector clicks is recorded with the actual relative frequencies \tilde{p}_{mn} is the *likelihood* $\mathcal{L}(\rho)$. Its logarithm is

$$\log(\mathcal{L}(\rho)) = N \sum_{m,n=0}^3 \tilde{p}_{mn} \log p_{mn}, \quad (23)$$

where the unknown intrinsic probabilities p_{mn} derive from the true statistical operator ρ that we wish to estimate. In the *maximum likelihood* (ML) strategy we take the ρ for which $\mathcal{L}(\rho)$ is largest as our best guess for the true ρ ,

$$\mathcal{L}(\rho_{\text{est}}) = \max_{\rho} \mathcal{L}(\rho). \quad (24)$$

The ML estimate is identical with the respective RD estimate of (22) if the RD estimate is permissible, that is: if there is a physical ρ whose probabilities are equal to the recorded relative frequencies. Accordingly, we need to calculate the ML estimate only if the RD reconstruction (22) fails.

The ML estimate is found by a numerical iteration that begins with an arbitrary guess $\rho_{\text{est}}^{(0)}$, for which the completely mixed state $\rho_{\text{est}}^{(0)} = 1/4$ is an option, and then determines improved estimates successively in accordance with the update rule

$$\rho_{\text{est}}^{(k+1)} = \frac{[1 + \epsilon_k R_k] \rho_{\text{est}}^{(k)} [1 + \epsilon_k R_k]}{\text{tr}\{[1 + \epsilon_k R_k] \rho_{\text{est}}^{(k)} [1 + \epsilon_k R_k]\}}, \quad (25)$$

where (replace Π_{mn} by T_{mn} for the product POM)

$$R_k = \sum_{m,n=0}^3 \frac{\tilde{p}_{mn} \Pi_{mn}}{\text{tr}\{\rho_{\text{est}}^{(k)} \Pi_{mn}\}} - 1 \quad (26)$$

and $\epsilon_k > 0$ is a suitably chosen increment (see below). The iteration stops when the trace class distance $\text{tr}\{|R_k \rho_{\text{est}}^{(k)}|\}$ is below the pre-set accuracy threshold. The rule (25), which is a variant of the recipe given in chapter 3 of [14], is such that all $\rho_{\text{est}}^{(k)}$ s are assuredly positive and normalized to unit trace.

In a bit of detail, the important steps of the iteration are as follows.

Given $\rho_{\text{est}}^{(k)}$,

- i. Compute R_k ; terminate the iteration if $\text{tr}\{|R_k \rho_{\text{est}}^{(k)}|\}$ is below the accuracy threshold, otherwise proceed.

- ii. Use two trial values for ϵ_k to compute two $\rho_{\text{est}}^{(k+1)}$ s and determine the value of the likelihood $\mathcal{L}(\rho_{\text{est}}^{(k+1)})$ for both.
- iii. Combine these two with the $\epsilon_k = 0$ value $\mathcal{L}(\rho_{\text{est}}^{(k)})$ and compute a quadratic function of ϵ_k that interpolates between the three support values.
- iv. Find the ϵ_k value for which the quadratic function assumes its maximum.
- v. Use this maximizing ϵ_k in (25) for the update $\rho_{\text{est}}^{(k)} \rightarrow \rho_{\text{est}}^{(k+1)}$.
- vi. Repeat.

With the optimization of ϵ_k in steps **ii–iv**, convergence is quite fast in practice.

5. Choosing states at random

For the simulated state tomography, we choose the true states either specifically or at random. We generate the random states by a procedure described in Refs. [13, 15]. A random rank- r state ρ is selected by first populating the entries of a $4 \times r$ matrix Y such that the real and imaginary parts follow noncentral Gaussian distributions offset by mean values given by the matrix $M = E(Y)$. Then

$$\rho = (|00\rangle, |01\rangle, |10\rangle, |11\rangle) \frac{YY^\dagger}{\text{tr}\{YY^\dagger\}} \begin{pmatrix} \langle 00| \\ \langle 01| \\ \langle 10| \\ \langle 11| \end{pmatrix} \quad (27)$$

is a rank- r state in the random sample that is characterized by matrix M . The choice $M = 0$ for $r = 4$ gives a uniform sample with respect to the Hilbert–Schmidt distance, by other choices we can regulate the average purity of the states in the random sample.

Random samples of pure states ($r = 1$) are unitarily invariant and thus uniform. So are random samples of unbiased mixed states ($M = 0$), but if we choose $M \neq 0$ for a mixed states sample, there will be a bias because we lose the unitary equivalence. The average performance of the SIC POM will depend on the sample or, equivalently, which one of the unitarily equivalent SIC POMs we use for the same biased sample.

Once the true state ρ is chosen for the simulation, we use the resulting quantum probabilities in conjunction with a standard (pseudo-)random number generator to get a total of N simulated detector clicks. The relative frequencies \tilde{p}_{mn} of detector clicks then determine the RD estimate of ρ and, if need be, also the ML estimate. The quality of the estimate is judged by the trace-class distance,

$$D = \frac{1}{2} \text{tr}\{|\rho - \rho_{\text{est}}|\}, \quad (28)$$

with $0 \leq D \leq 1$. We have $D = 0$ only if the two states are equal, $\rho_{\text{est}} = \rho$, and the maximal distance $D = 1$ when they are orthogonal $\rho_{\text{est}}\rho = 0$. Typically, the distance decreases $D \propto N^{-1/2}$ as the sample size N increases.

6. Tomography of maximally entangled pure states

We now compare the tomographic performances of RD and ML reconstruction for pure states for which the failure of RD estimation is typical rather than exceptional. In particular, we choose as the true states the four standard Bell states that are given by

$$\begin{aligned} \rho_0 &= \frac{1}{2}(1 - \sigma_x \otimes \sigma_x - \sigma_y \otimes \sigma_y - \sigma_z \otimes \sigma_z) = |\Psi^-\rangle\langle\Psi^-|, \\ \rho_x &= \frac{1}{2}(1 - \sigma_x \otimes \sigma_x + \sigma_y \otimes \sigma_y + \sigma_z \otimes \sigma_z) = |\Phi^-\rangle\langle\Phi^-|, \\ \rho_y &= \frac{1}{2}(1 + \sigma_x \otimes \sigma_x - \sigma_y \otimes \sigma_y + \sigma_z \otimes \sigma_z) = |\Phi^+\rangle\langle\Phi^+|, \\ \rho_z &= \frac{1}{2}(1 + \sigma_x \otimes \sigma_x + \sigma_y \otimes \sigma_y - \sigma_z \otimes \sigma_z) = |\Psi^+\rangle\langle\Psi^+| \end{aligned} \quad (29)$$

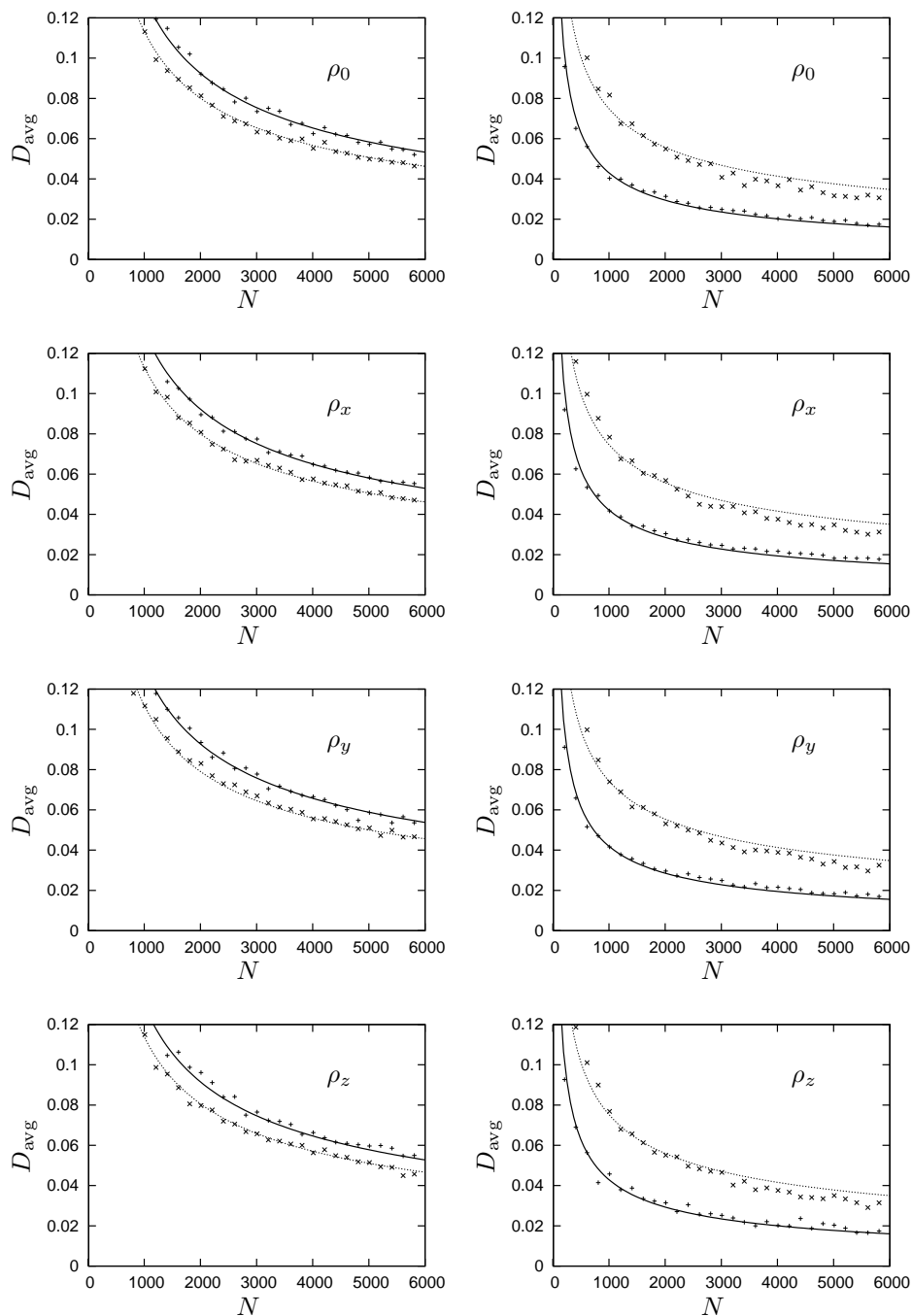


Figure 1: Simulated tomography of two-qubit Bell states with the product POM (crosses + and solid line) or the SIC POM (crosses x and dotted line) with raw-data state estimation (left-side plots) and maximum-likelihood state estimation (right-side plots). The trace-class distance D_{avg} is averaged over a hundred simulation runs with up to 6000 measured qubit pairs, all prepared in the respective Bell state. The solid and dotted lines are least-square fits to a power law $D_{\text{avg}} = a/N^c$.

with

$$|\Psi^\pm\rangle = \frac{1}{\sqrt{2}}(|01\rangle \pm |10\rangle) \quad \text{and} \quad |\Phi^\pm\rangle = \frac{1}{\sqrt{2}}(|00\rangle \pm |11\rangle). \quad (30)$$

The plots in the left column of Fig. 1 show the N dependence of the distance between the RD estimate and the respective Bell state. Not unexpectedly, the SIC POM outperforms the product POM. But this observation is, in fact, misleading as almost all RD estimates are unphysical. The comparison with the ML estimates in the right column is more to the point, and there the picture is reversed: rather unexpectedly, the product POM gives better estimates than the SIC POM.

The simulated product-POM data compare well with the experimental data of Ref. [8], where a RD estimate was used. The experimental values for the average trace-class distance D_{avg} showed a dependence $\propto N^{-1/2}$ on the total number of detector clicks, and our simulated data follow the same reciprocal square-root law.

The striking similarity among the four plots of each column in Fig. 1 is not accidental but could in fact have been anticipated. The transformations effected by the squares of the Heisenberg–Weyl operators X and Z of (20) interchange the Bell states,

$$X^2\rho_0X^2 = \rho_x, \quad Z^2\rho_xZ^2 = \rho_y, \quad X^2\rho_yX^2 = \rho_z, \quad Z^2\rho_zZ^2 = \rho_0, \quad (31)$$

where $X^2 = \sigma_x \otimes 1$ and $Z^2 = 1 \otimes \sigma_z$ act on one of the qubits only. It follows that the respective sets of probabilities p_{mn} of the Bell states are permutations of each other.

For a more systematic quantitative comparison between the product POM and the SIC POM, we introduce a *performance factor* η , guided by the usual understanding of optimal tomography with SIC POMs. Suppose the power laws have the form $D = a/N^c$, and $N^{(\text{prod})}$ and $N^{(\text{SIC})}$ are the respective number of qubit pairs that need to be measured to reach the desired threshold value D_{thr} . Then

$$\eta = \frac{N^{(\text{prod})}}{N^{(\text{SIC})}} = \left(\frac{a^{(\text{prod})}}{D_{\text{thr}}} \right)^{1/c^{(\text{prod})}} \left(\frac{D_{\text{thr}}}{a^{(\text{SIC})}} \right)^{1/c^{(\text{SIC})}} \quad (32)$$

defines η . For $\eta > 1$, the larger its value, the faster the convergence rate of the SIC POM power law compared to that of the product POM for a fixed benchmark distance D_{thr} . Similarly, $\eta < 1$ indicates that the product POM is more efficient.

From top to bottom, the η values for the data in Fig. 1 are 1.32, 1.31, 1.37, and 1.29 for the RD estimates of the left column, and 0.42, 0.43, 0.41, and 0.42 for the ML estimates of the right column, all referring to the benchmark value $D_{\text{thr}} = 0.1$. It is staggering how much better the product POM performs as soon as proper ML estimation of the state is incorporated. This observation is not limited to the maximally entangled Bell states. We have seen it also for quite a few randomly chosen pure two-qubit states and for the three-qubit W state $|W\rangle = (|001\rangle + |010\rangle + |100\rangle)/\sqrt{3}$. A more extensive study of three-qubit tomography appears to be worthwhile.

That said, we must also note that the four Bell states of (29) are not typical among the maximally entangled states, owing to their particular alignment with the outcomes of the two POMs under consideration. When one averages over a large sample of maximally entangled states, see the bottom right subtable in Table 1, the picture is different: the average η value is a bit larger than 1.

7. Averaged performances

The data for average performances of the product POM and the SIC POM for randomly chosen states are collected in Table 1. As explained in the table caption, we report data for four samples of random states: an unbiased set of mixed states, a biased high-purity set of mixed states, a set of pure states, and a sample of maximally entangled states.

The standard deviation for each quantity, as listed in Table 1, is a combination of two types of errors: one that comes from performing a number of experiments on a fixed state and another incurred as we sample the random states. To identify the two different errors, one would need to perform an extremely large number

Table 1: Average values for three samples of 1000 randomly chosen states each. The top left table is for unbiased full-rank mixed states ($r = 4$ and $M = 0$ in Sec. 5); the top right table is for biased full-rank mixed states ($r = 4$ and $M \neq 0$) whose purity $\text{tr}\{\rho^2\}$ exceeds 0.8 with high probability. The bottom left table is for pure states ($r = 1$); the bottom right table is for maximally entangled states. In each table, the first and second rows report the average number of qubit pairs that need to be measured before the benchmark value of $D_{\text{thr}} = 0.1$ is reached, for raw-data state estimation (RD) and maximum-likelihood estimation (ML) as well as for the product POM and for the SIC POM. The third rows show the performance factors η of (32) that compares the efficiency of the two POMs. For the more relevant ML estimation, there is no significant advantage of the SIC POM over the product POM, except perhaps for the sample of unbiased mixed states which is dominated by low-purity states [15].

Unbiased mixed states			Biased mixed states		
	RD	ML		RD	ML
prod	1787 ± 102	1534 ± 156	prod	1739 ± 114	712 ± 99
SIC	1349 ± 67	1165 ± 101	SIC	1293 ± 67	639 ± 73
η	1.33 ± 0.09	1.32 ± 0.11	η	1.35 ± 0.11	1.12 ± 0.16

Pure states			Maximally entangled states		
	RD	ML		RD	ML
prod	1738 ± 118	472 ± 73	prod	1728 ± 103	552 ± 89
SIC	1284 ± 70	455 ± 108	SIC	1276 ± 70	442 ± 72
η	1.35 ± 0.16	1.09 ± 0.29	η	1.36 ± 0.11	1.27 ± 0.29

of simulated experiments, in excess of 10,000, on each state and so reduce the former error to orders of magnitude smaller than the latter error.

One lesson of the numbers in Table 1 is that the RD estimate is not only sometimes unacceptable, but it also performs worse than the ML estimate. Clearly, one should not rely at all on the RD estimate.

The second lesson is that there is no significant difference between the efficiency of the SIC POM and the product POM for states of high purity, and there is not much of an advantage for the SIC POM when the states have low purity. The averages over samples of randomly chosen states do not confirm the observation made for Bell states in Sec. 6.

8. Conclusion

We have carried out a numerical study that compares the performance of the product POM and the SIC POM in qubit-pair tomography. All evidence indicates that the product POM performs almost as well as the SIC POM; there is not much of an advantage in employing the SIC POM. Since it is much more challenging to realize the SIC POM in a laboratory experiment than the product POM, we conclude that the implementation of the SIC POM for tomographic purposes is hardly worth the trouble.

Acknowledgments

Centre for Quantum Technologies is a Research Centre of Excellence funded by Ministry of Education and National Research Foundation of Singapore.

References

- [1] G. Zauner, Ph.D. thesis, University of Vienna, 1999. Available online at <http://www.mat.univie.ac.at/~neum/papers/phypapers.html>
- [2] J.M. Renes, R. Blume-Kohout, A.J. Scott, and C.M. Caves, J. Math. Phys. **45**, 2171 (2004).
- [3] J. Řeháček, B.-G. Englert, and D. Kaszlikowski, Phys. Rev. A **70**, 052321 (2004).
- [4] D.M. Appleby, H.B. Dang, and C.A. Fuchs, eprint arXiv:0707.2071 [quant-ph] (2007).

- [5] B.-G. Englert, K.M. Tin, C.G. Goh, and H.K. Ng, *Laser Physics* **15**, 7 (2005).
- [6] A. Ling, K.P. Soh, A. Lamas-Linares, and C. Kurtsiefer, *J. Mod. Opt.* **53**, 1523 (2006).
- [7] A. Ling, K.P. Soh, A. Lamas-Linares, and C. Kurtsiefer, *Phys. Rev. A* **74**, 022309 (2006).
- [8] A. Ling, A. Lamas-Linares, and C. Kurtsiefer, eprint arXiv:0807.0991 [quant-ph] (2008).
- [9] H. Zhu, Y.S. Teo, and B.-G. Englert, eprint arXiv:0906.3985 [quant-ph] (2009).
- [10] B.-G. Englert, D. Kaszlikowski, H.K. Ng, W.K. Chua, J. Řeháček, and J. Anders, eprint arXiv:quant-ph/0412075 (2004).
- [11] H. Zhu, Y.S. Teo, and B.-G. Englert, *Structures of Two-Qubit SIC POMs* (in preparation).
- [12] D.M. Appleby, *J. Math. Phys.* **46**, 052107 (2005).
- [13] K. Życzkowski and H.J. Sommers, *J. Phys. A: Math. Gen.* **34**, 7111 (2001).
- [14] *Quantum State Estimation*, edited by M. Paris and J. Řeháček, *Lecture Notes in Physics*, Vol. 649 (Springer, Berlin 2004).
- [15] I. Bengtsson and K. Życzkowski, *Geometry of Quantum States — An Introduction to Quantum Entanglement* (Cambridge University Press 2006).